Field measurements of the energy delivered to the channel bed by moving bed load and links to bedrock erosion

Jens M. Turowski,[1,2] Martin Böckli,[1] Dieter Rickenmann,[1] and Alexander R. Beer[1]

Received 15 February 2013; revised 11 November 2013; accepted 12 November 2013; published 9 December 2013.

[1] Impact-driven fluvial erosion is directly related to the energy delivered to the channel bed by moving bed load. Using a novel protocol, we have measured this energy in four mountain streams in Austria and Switzerland. Similar to bed load transport rates, the energy delivered to the bed displays large scatter over several orders of magnitude even for a constant discharge. We found that only a small fraction (<1%) of the total energy available to the stream is delivered to the bed and can be used for erosive work. Empirical predictive equations can be defined for specific sites, but there is large site-to-site variability. Prediction of energy delivered to the bed using the saltation-abrasion model of bedrock erosion only provides the observed trends when measured bed load transport rates are used as input. Using an empirical transport law calibrated to the conditions at one of the study streams leads to overprediction of delivered energies by more than 2 orders of magnitude. This overprediction decreases with increasing discharge, and thus, at high discharges, better predictive results are obtained. We find a correlation between the channels' bed slope or characteristic grain sizes of the channel bed and the fraction of energy delivered to the bed of the total energy available to the stream. This observation provides a tentative link between fundamental fluvial incision processes to the stream power model family that has widely been used to model fluvial bedrock incision in landscape evolution simulations.

Citation: Turowski, J. M., M. Böckli, D. Rickenmann, and A. R. Beer (2013), Field measurements of the energy delivered to the channel bed by moving bed load and links to bedrock erosion, *J. Geophys. Res. Earth Surf.*, *118*, 2438–2450, doi:10.1002/2013JF002765.

1. Introduction

[2] Fluvial bedrock erosion is a key process in evolving orogens. Bedrock channels modulate the coupling between climate, tectonics, and erosion, by cutting into the underlying substrate, steepening adjacent hillslopes, and by evacuating the sediment produced in the landscape [e.g., *Whipple et al.*, 2000; *Hovius and Stark*, 2006; *Turowski*, 2012]. A detailed knowledge of fluvial bedrock erosion processes is important not only for the comprehension of channel dynamics, sediment transport, and channel-hillslope coupling but can affect our understanding of the rates of evolution of whole mountain belts [e.g., *Egholm et al.*, 2013].

[3] In many streams that are actively eroding bedrock, impact wear is thought to be the dominant process of incision [e.g., *Whipple et al.*, 2000; *Hartshorn et al.*, 2002; *Sklar and Dietrich*, 2004; *Cook et al.*, 2013; *Wilson et al.*, 2013]. Moving sediment particles impact exposed rock surfaces and erode the rock [e.g., *Gilbert*, 1877; *Moore*, 1926; *Sklar and Dietrich*, 2001; *Turowski et al.*, 2007; *Johnson and Whipple*, 2007, 2010]. In the classic impact wear model of *Bitter* [1963a, 1963b], the average volume of rock V_i removed by a single particle impact is linearly related to the kinetic energy transferred by the impacting grains (see also *Head and Harr* [1970] and *Momber* [2004]). This can be encapsulated in the equation

$$V_i = \frac{E_g - \varepsilon_t}{E_V} \tag{1}$$

[4] Here E_g is the energy transferred to the rock by the impact of a single grain, ε_t is an erosion threshold, and E_V is the energy per unit volume needed to remove the rock. *Sklar and Dietrich* [2004] adapted *Bitter*'s [1963a, 1963b] equations for fluvial bedrock abrasion by saltating bed load and argued based on laboratory experiments [*Sklar and Dietrich*, 2001] that the erosion threshold is negligible. Thus, we can write for impact-driven fluvial bedrock abrasion

$$V_i = \frac{E_g}{E_V} \tag{2}$$

[5] As is clear from equation (2), the volume of rock removed by impact erosion is directly proportional to the energy delivered to the bed. The energy delivered to the bed E_g and the constant of proportionality E_V have been linked

[1]Swiss Federal Research Institute WSL, Birmensdorf, Switzerland.
[2]Helmholtz Centre Potsdam, GFZ German Research Centre for Geosciences, Potsdam, Germany.

Corresponding author: J. M. Turowski, Swiss Federal Research Institute WSL, Zürcherstrasse 111, CH-8903 Birmensdorf, Zuerich Switzerland. (turowski@gfz-potsdam.de)

2169-9003/13/10.1002/2013JF002765

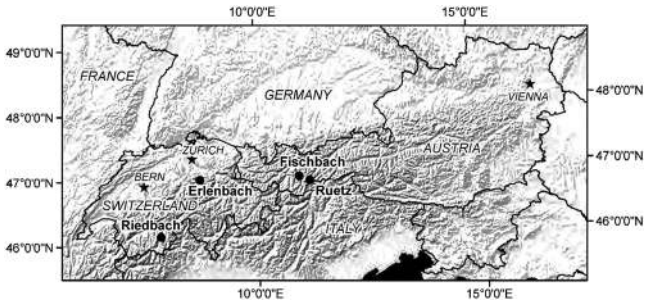

Figure 1. Location map of the study sites in Switzerland and Austria.

to hydraulics and rock properties using theoretical and semi-empirical arguments [*Sklar and Dietrich*, 2004] and calibrated on experimental data from an erosion mill [*Sklar and Dietrich*, 2001]. However, direct field measurements of the relevant parameters are not yet available. The aims of the present article are twofold. First, we introduce a novel field technique to directly measure in the field the energy delivered to the bed by moving bed load using a bed load surrogate monitoring system, employed in several alpine mountain streams [*Rickenmann and McArdell*, 2007; *Turowski and Rickenmann*, 2011; *Turowski et al*., 2011]. The system is known in the literature as Swiss plate geophone system [e.g., *Gray et al*., 2010] and is herein referred to as geophone sensor system. We calibrated the sensor output in the laboratory to obtain absolute energy values from single impacts. Second, we describe field measurements from four mountain streams and compare the data of one these streams to theoretical predictions of the delivered energy using a mechanistic erosion model [*Sklar and Dietrich*, 2004]. We use the results to discuss links to popular bedrock erosion models from the literature, namely, the stream power model [*Seidl et al*., 1994] and the saltation-abrasion model [*Sklar and Dietrich*, 2004].

2. Field Sites

[6] The energy delivered to the bed by moving gravel was measured in four streams in the European Alps (Figures 1 and 2; Table 1). All four streams are gravel-bed rivers, and the main aim of the sensor installation was the long-term observation of bed load transport, partly for scientific and partly for operational reasons.

[7] The main observation site is the Erlenbach, an experimental catchment operated by the Swiss Federal Research Institute WSL [*Hegg et al*., 2006]. It is located in the Alptal valley (canton Schwyz) in the Swiss preAlps. The gauging station is located at an elevation of 1110 MASL, where the Erlenbach stream drains a total area of 0.7 km^2. Floods occur mainly due to thunderstorm events during the summer. The catchment is well instrumented for sediment transport observations and is described in detail elsewhere [*Rickenmann and McArdell*, 2007; *Turowski et al*., 2009; *Rickenmann et al*., 2012]. Six geophone sensors are located in a check dam upstream of a sediment retention basin and in close proximity to the discharge gauge (Figure 2a; only the six plates in the channel center are instrumented). Although the sensors have been in operation since 1986, the necessary data to calculate energy delivery have only been recorded together with stage level at 1 min intervals since 4 July 2011. Data used here were recorded from July to December 2011. Throughout the present paper, we focus on an Erlenbach bed load transport event in October 2011 with a peak discharge of 1130 l/s as an example. The event was selected because it featured the largest discharge peak in the studied period.

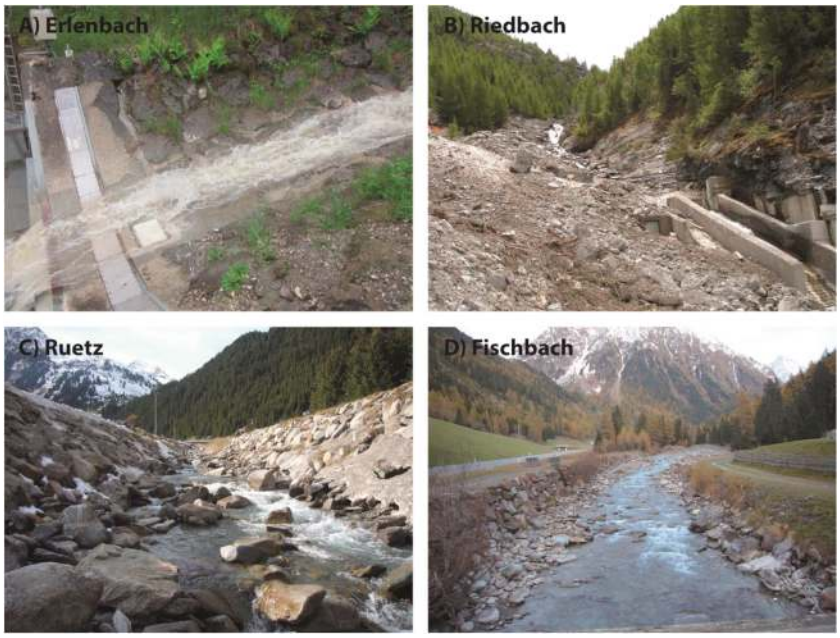

Figure 2. Pictures of the stream. (a) Erlenbach shoot channel and geophone sensor plates in the cross section. (b) Gaging station and channel at the Riedbach. (c) View of the channel directly upstream of the survey site at the Ruetz. (d) View of the channel directly upstream of the survey site at the Fischbach.

Table 1. Stream Characteristics

	Erlenbach	Fischbach	Riedbach	Ruetz
Location	Alptal, Schwyz, Switzerland	Tyrolia, Austria	Grächen, Vallais, Switzerland	Tyrolia, Austria
Measurement period	July 2011–Dec. 2011	Jan 201–June 2011	Aug 2008–Sep 2011	April 2010–June 2011
Recording interval (min)	1	15	10	15
Elevation (MASL)	1110	1540	1809	1684
Drainage area (km^2)	0.7	71	15.8	28
% of glaciation	0	17	53	22
Mean discharge (m^3/s)	0.034	31.1	0.71	53.7
Channel bed slope	0.15[a]	0.02	0.40	0.06
Flow width (m)	1.2[a]	9.5	3.5	8.5
D_{50} (cm)	9.6	3.8	38.5	6.3
D_{90} (cm)	48	20	110	40

[a]Channel bed slope and flow width of the Erlenbach differ from previously published values here, because they relate to an artificial shoot upstream of the geophone sensor plates, rather than the natural channel bed.

[8] The Riedbach near Grächen in the Matter Valley in Switzerland is a steep, glacially fed stream [*Nitsche et al*., 2012]. Discharge is gauged at an elevation of 1809 MASL, at a water intake for a hydropower station, where the stream drains a total area of 15.8 km^2, 53 % of which is glaciated. A row of seven instrumented geophone sensor plates is installed across the stream at the gauging station upstream of a tyrolean weir (Figure 2b). Discharge and sediment transport data are recorded at 10 min intervals. The data used here were recorded from August 2008 to September 2011.

[9] The observation site at the Ruetz in the Stubai Valley in Austria is located at an elevation of 1684 MASL in the high Alps (Figure 2c), where the stream drains a total area of 28 km^2, ~22 % of which is glaciated. During the summer months, discharge is consistently high due to glacial melt, and bed load transport occurs more or less continuously. A similar situation as to the Ruetz pertains to the Fischbach in the Ötz Valley in Austria, which at the observation site at 1540 MASL drains 71 km^2, 17 % of which is glaciated (Figure 2d). At both sites, eight geophone plates are active, and discharge and sediment transport data are recorded at 15 min intervals at the gauging stations operated by a hydro power company (see also *Turowski et al*. [2011]). The extent of the glaciated area in the Fischbach and Ruetz catchments is based on surveys from 1986 [*Hasslacher and Lanegger*, 1988] and has probably diminished since then. Data for the Fischbach used herein were recorded between January and June 2011 and for the Ruetz between April 2010 and June 2011.

3. Methods

3.1. Sensor System and Energy Calibration

[10] The WSL bed load surrogate monitoring system (Swiss plate geophone system) consists of steel plates with dimensions of 50 × 36 cm that are mounted flush with the stream bed. A commercially available geophone sensor (20DX geophone from Geospace Technologies, Houston, Texas, in a PC801 LPC Land-case) is fixed in the center under the plate. As bed load passes over the plate, vibrations occur, which are recorded by the sensor. The geophone system has been used for over a decade to monitor bed load transport in alpine catchments. For this purpose, the number of vibration intensity peaks above a predefined threshold (impulses) are counted, which are proportional to bed load volumes passing the sensor [*Rickenmann and McArdell*, 2007, 2008; *Rickenmann et al*., 2012]. More information on the geophone system can be found in the publications by *Rickenmann et al*. [2012, 2013], *Turowski and Rickenmann* [2009, 2011], and in the references cited therein. In each of the sites studied here, several steel plates are placed in a row across the stream, covering the whole cross section. In the Fischbach and the Ruetz, only every second plate is instrumented with a geophone, while in the Erlenbach, the six central plates are active, and the Riedbach every plate is instrumented.

[11] The geophone sensor consists of a coil, which can move in the field of a permanent magnet due to vibrations, such that the velocity vector is perpendicular to the magnetic flux density vector B. The induced voltage U_{ind} is then proportional to the velocity of the coil v.

$$U_{ind} = -dvB \tag{3}$$

[12] Here d is the distance between the magnetic poles. In the geophone system, the geophone sensor is aligned in such a way that the normal velocity of the vibrations in the center of the plate is measured. The kinetic energy of the coil is proportional to the velocity squared, and energy transferred to the sensor by moving bed load E_{bed} can thus be measured from the integrated squared signal of the geophone output U_g, which is proportional to U_{ind} but may be amplified.

$$E_{bed} = K\sum U_g^2 \tag{4}$$

[13] Here K is a constant, which we calibrated by laboratory experiments. To this end, a projectile ball was dropped onto various points of the sensor plate from known heights, and the response signal was recorded [*Böckli*, 2011]. The ball was made of hard rubber with a steel center and had a mass of $M_{\mathrm{imp}} = 0.144$ kg. For each drop height, we recorded five impact events with a high-speed camera at 500 frames per second. The films were used to measure impact velocity V_{imp} and rebound height h. The energy delivered to the sensor plate in the impact E_{bed} could then be calculated using the equation

$$E_{bed} = \frac{1}{2}M_{imp}V_{imp}^2 - gM_{imp}h \tag{5}$$

[14] Here g is the acceleration due to gravity. For each drop height, we thus obtained a relationship between delivered energy and drop height, which was used for all experiments.

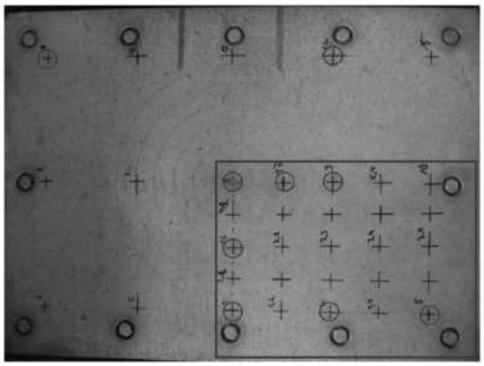

Figure 3. Top view photograph of a geophone sensor plate used for the laboratory experiments, with impact locations marked by black crosses. The quadrant on the lower right-hand side was studied in detail, and the assumption of symmetry was checked by measuring sensor response for selected points in the other quadrants. At circled impact locations, experiments were made for all drop heights. At all other impact locations, the sensor response was studied only for a drop height of 50 cm.

[15] Assuming that the sensor plate reacts symmetrically, we measured sensor response to impacts at 25 regularly spaced points in one quadrant of the sensor plate (Figure 3), repeating each experiment 10 times. We checked the assumption of symmetry with measurements at selected points in the other three quadrants. At seven of the 25 points, we measured the sensor's response to impacts from various drop heights. The minimum drop height was 10 cm and the maximum height 80 cm, with intermediate heights at a spacing of 10 cm. This corresponds to impact energies ranging from 0.05 J to 0.5 J. A different calibration relation between impact energy and the squared integrals of the sensor response was derived for each sensor point. Similar relations of nearby points were averaged, and the sensor plate was partitioned into five zones corresponding to different calibration relations (Figures 4a and 5). Assuming that each point on the sensor plate is equally likely to be impacted by moving bed load in the stream, the energy delivered to the whole plate was calculated by weighting the different calibration relations by the relative area of the respective zones on the plate. The resulting plate-averaged calibration relation is nearly linear and can be described by the equation (Figures 4b and 5):

$$E_{bed} = 0.0106\left(\sum U_g^2\right)^{1.06} \tag{6}$$

3.2. Treatment of Field Data

[16] In the field, the geophone sensor signal is recorded at a frequency of 10,000 Hz, and summary values (e.g., impulses, sum of the squared integrals) [see *Rickenmann et al*., 2012, 2013] are stored at the site-specific temporal resolution. The energy formula derived in the laboratory (equation 6) was applied to the squared integral of the sensor signal to obtain the energy delivered to the bed by the stream. To exclude noise of the sensor system, for example due to flowing water, we considered time steps only when a minimum number of impulses were recorded, implying that coarse bed load was transported. For the Erlenbach, this impulse threshold was specified as one impulse per minute for each sensor plate. Using the calibration factor for material larger than 20 mm [*Rickenmann et al*., 2013], this corresponds to a bed load mass of 0.19 kg or a transport rate per unit width of 6.33×10^{-3} kg m^{-1} s^{-1}. To allow comparison between the streams, we used the latter as a threshold transport rate in all streams. For the Riedbach, this corresponds to a minimum number of 21 impulses in a measurement period (10 min), for the Fischbach to 66 impulses, and for the Ruetz to 47 impulses (both in 15 min). For all studied streams, the specified threshold reasonably filters out measurements at unplausibly low discharges. The measured energy values at the Fischbach and the Ruetz additionally need to be doubled for analysis, because only every second sensor plate is instrumented there.

[17] To obtain total stream energies, we calculated stream power Ω and multiplied by the length of the measurement time step Δt and the along-stream length of the geophone sensor plate $L = 0.36$m. The total energy of the stream E_{tot} is then given by

$$E_{tot} = g\rho QSL\Delta t = \Omega L\Delta t \tag{7}$$

[18] Here ρ is the density of water, Q is the discharge, and S is the channel bed slope. Throughout the paper, we will frequently use the ratio of the energy delivered to the bed to the total stream energy, hereafter referred to as the energy-delivery ratio and abbreviated by $R = E_{bed}/E_{tot}$.

[19] Grain size distributions were measured with the line-by-number method [*Fehr*, 1987], while slope was measured with a hand-held inclinometer over a distance of ~100 m upstream of the measurement cross section at the Fischbach, Riedbach, and Ruetz and from survey data at the Erlenbach. For additional details, see *Turowski et al*. [2011].

3.3. Theoretical Calculation of the Energy Delivered to the Bed

[20] In this section, we compare the energy values measured in the field to calculations using an equation that is a

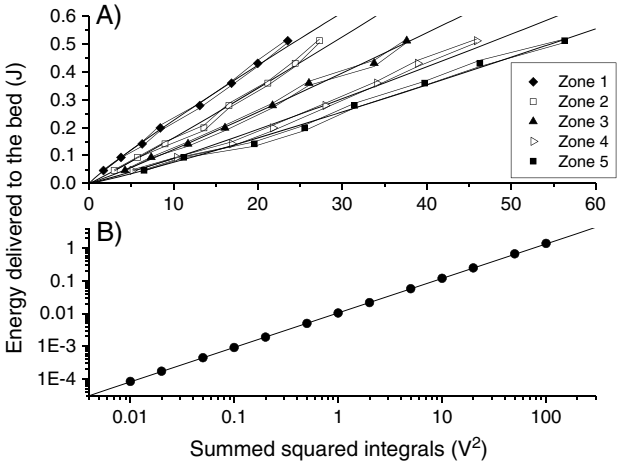

Figure 4. (a) Relationship between impact energy (equation 5) and squared integrals from the impact experiments for each of the five sensor zones. (b) Averaged calibration for the five sensor zones (see Figure 5).

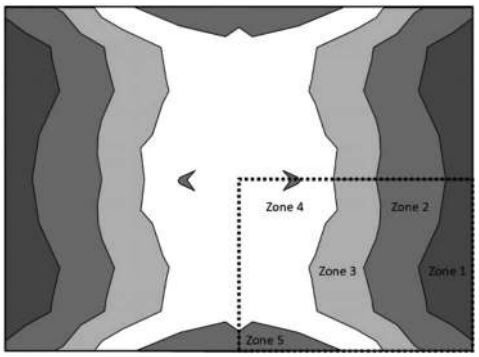

Figure 5. Five zones of the sensor plate with similar response to impacts.

component of the saltation-abrasion model for bedrock erosion [*Sklar and Dietrich*, 2004]. The saltation-abrasion model is built on the assumption that the volume of bedrock removed by a single impact is proportional to the energy of the impactor at the moment of impact [see *Sklar and Dietrich*, 2004, equation (3)] (the threshold is neglected by them). Note the model does not work with the energy delivered to the bed but with the total kinetic energy of the impactors, including energy retained by the impactor in the rebound [see *Sklar and Dietrich*, 2004, equation (3)]. The discrepancy between this formulation and the actual energy delivered to the bed is subsumed into the rock resistance coefficient, which is an empirical, laboratory-calibrated scaling factor. To obtain the energy of the impactors E_{kin}, the saltation-abrasion model equation [*Sklar and Dietrich*, 2004, equation (24a)] needs to be multiplied by the total energy required to erode a unit volume of rock (defined in *Sklar and Dietrich* [2004, equation (4)]), yielding the equation (note that *Sklar and Dietrich* [2004] used the symbol E for erosion rate, while we use it for energy)

$$E_{kin} = 0.04\left(\frac{\rho_s}{\rho} - 1\right) g q_s \left(\frac{\tau}{\tau_c} - 1\right)^{-1/2} \tag{8}$$

[21] Here q_s is the mass bed load transport rate per unit width, ρ_s is the density of the sediment, $\tau = \rho g H S$ is the shear stress on the bed, τ_c the critical shear stress for the onset of bed load motion, and H is the hydraulic radius of the flow. We used a value of $\tau_c = 102.6$ Pa for the critical shear stress (equivalent to a shields stress of 0.066 for the median grain size), which corresponds to the measured onset of bed load transport in the October 2011 event. In equation (8), we neglected the cover effect and the suspension effect term [see *Sklar and Dietrich*, 2004, equation (24a)]. For efficient measurements, the geophone systems are installed in such a way that sediment covering of the sensors is extremely unlikely, thus, the stream behavior on-site is tools dominated, and the cover effect can be neglected to first approximation. The suspension effect term is negligible for $\tau < 10\ \tau_c$, which is commonly the case [*Sklar and Dietrich*, 2004; see also *Lamb et al*., 2008]. To obtain absolute energy values, equation (8) needs to be multiplied by the area of the geophone sensor plate, the number of sensors in the cross section, and the length of the time step.

[22] For calculating energy values with equation 8, information on bed load transport rates is necessary. We used (i) the transport rates determined with the geophone sensors (method 1) and (ii) transport rates estimated using a power law function of discharge as put forward by *Barry et al*. [2004] (method 2).

$$Q_s = k_B Q^{\beta} \tag{9}$$

where k_B and β can be estimated with the method of *Barry et al*. [2004] with the following equations:

$$\beta = -2.45 q^* + 3.56 \tag{10}$$

[23] The dimensionless bed load transport ratio q^* is given by the equation:

$$q^* = \left(\frac{\tau_{Q_2} - \tau_{d_{50s}}}{\tau_{Q_2} - \tau_{d_{50ss}}}\right)^{1.5} \tag{11}$$

[24] Here $\tau_{Q_2} = 93$ Pa is the bed shear stress during a 2 year flood, $\tau_{d_{50s}} = 58.3$ Pa is the critical shear stress necessary to move the median grain size of the surface material, and $\tau_{d_{50ss}} = 11.7$ Pa is the critical shear stress necessary to move the median grain size of the subsurface material, which is assumed to be equal to the median grain size of material deposited in the retention basin [see *Rickenmann and McArdell*, 2007]. The power function of *Barry et al*. [2004] is advantageous for our purpose in comparison to more commonly used formulae, since it is calibrated on field data and predicts actual bed load transport rates rather than transport capacity. Using equations (10) and (11), we obtained $\beta = 2.88$. Note that the correction published by *Barry et al*. [2007] is not relevant here, as it only affects the estimation of the prefactor, which we obtained from site-specific data as follows. Many commonly used bed load equations show poor predictive performance for steep streams such as the Erlenbach [e.g., *Nitsche et al*., 2011; *Yager et al*., 2012]. Thus, the prefactor of the power law was calibrated at $0.51\mathrm{m}^{-5.64}\,\mathrm{s}^{1.88}$ using data from the Erlenbach instead of using *Barry et al*.'*s* [2004] equation, in order to obtain the correct order of magnitude of sediment supply. To this end, *Barry et al*.'*s* [2004] power equation was applied to the Erlenbach discharge time series since 1983, and the prefactor was adjusted in such a way that the measured accumulated sediment volumes in the retention basin were correctly predicted.

4. Results

4.1. Energy Delivery During a Transport Event at the Erlenbach

[25] The transport event described here occurred on 10 October 2011 in the Erlenbach after some moderate rainfall (Figure 6a). With a peak discharge of 1130 l/s, it is a comparatively small event for the Erlenbach. Similarly sized events typically occur several times per year. Nevertheless, the peak featured the largest discharge observed in the studied period. Bed load transport was registered more or less continuously for a period spanning 11 h starting around 2:30 A.M. Over the event, the stream delivered 206 J to the channel bed, out of a total energy of ~34,000 J (Figure 6b). Thus, only

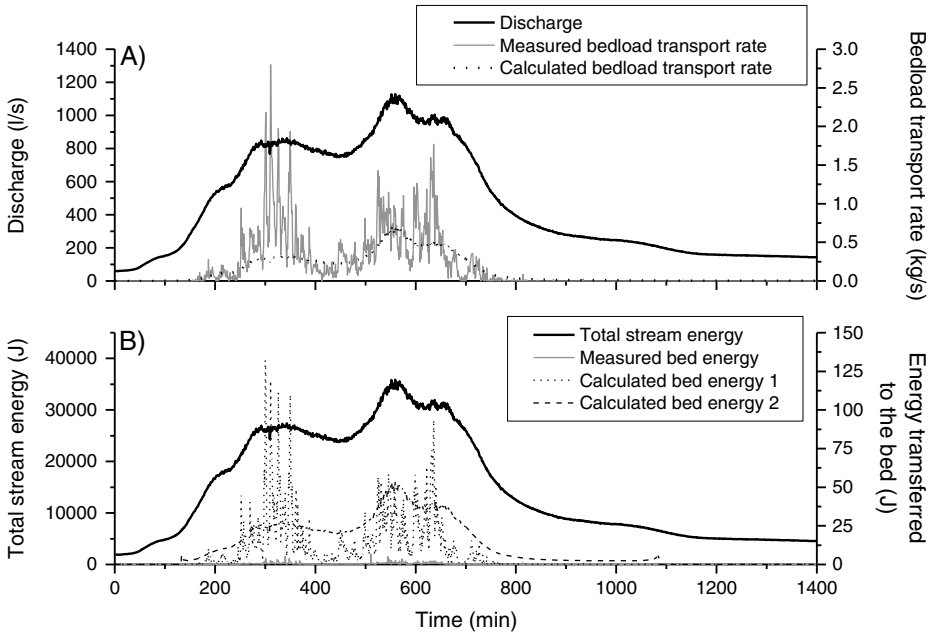

Figure 6. Hydraulic and energy characteristics of the bed load transport event in the Erlenbach on 10 October 2011. (a) Discharge and resulting bed load transport obtained from measurement and calculation with the equation of *Barry et al*. [2004]. (b) Total stream energy and transferred energy to the bed. The latter was calculated using equation (8) with two different methods: (1) measured bed load transport rate and (2) the empirical bed load transport model calibrated to the long-term sediment delivery at the Erlenbach.

0.6% of the energy available to the stream was delivered to the bed and could have been expended for eroding bedrock.

[26] Both bed load transport rates and the measured energy transferred to the bed fluctuate strongly over the course of a flood event, even at times when discharge varies slowly. The bed load transport rates, energy, and the energy-delivery ratio are correlated to discharge (Figure 7), but at a given discharge, scatter can range over more than 2 orders of magnitude.

4.2. Energy Delivery as a Function of Catchment Parameters

[27] The measured energy transferred to the bed can be related to the total energy of the stream (Figure 8). For a given observation, site total stream energy is proportional to discharge but varies from site to site due to the influence of channel bed slope (equation 7). For the Riedbach and Fischbach, a trend between these variables is not obvious, although it is hinted at in the Fischbach data. For the Erlenbach and Ruetz, a trend is visible. The discrepancy may be due to the different range of discharges covered by the data, spanning less than an order of magnitude in total stream energy for the Riedbach and Fischbach. For the Erlenbach and the Ruetz, the discharge range spans just over an order of magnitude.

[28] The long-term energy-delivery ratio R_{LT} (calculated as delivered energy to the bed by bed load E_{bed} over the measurement period divided by total stream energy over the measurements period E_{tot}) and the mean energy-delivery ratio R_M (calculated as the mean of the energy-delivery ratios for each of the individual measurements) can be expected to be related to main catchment properties such as drainage area, sediment availability, magnitudes/characteristics of discharge, channel bed slope, or grain size characteristics. We could not find a convincing correlation with tested parameters including drainage area, mean discharge, and mean discharge per unit width over the survey period, channel bed slope, and grain size characteristics for the R_M (Figure 9). The long-term ratio

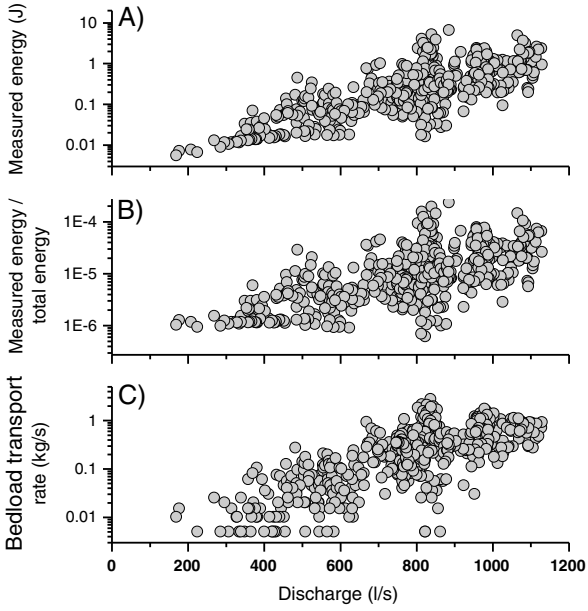

Figure 7. Functional relation to discharge of (a) the measured energy delivered to the stream bed, (b) the ratio of energy delivered to the bed to the total stream energy R, and (c) the measured bed load transport rate. All data are from 1 min measurements for the Erlenbach event of October 2011.

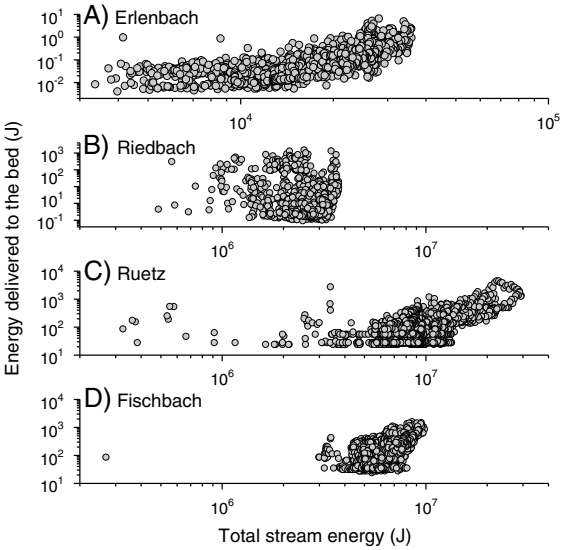

Figure 8. Energy delivered to the bed as function of total stream energy for the whole measurements periods for the four streams. (a) Erlenbach, (b) Riedbach, (c) Ruetz, and (d) Fischbach.

R_{LT} is anticorrelated with channel bed slope, median grain size D_{50}, and the grain size larger than 90% of the grains D_{90}.

5. Discussion

5.1. Sensor Calibration and Error Estimation

[29] Measurement errors in the laboratory calibration of individual points on the sensor plate are small, since the impact energy can be measured with high accuracy and the sensor response is stable over time. Small errors may arise because different vibration modes of the plate may be excited when impacting particles consist of a different material than used in the lab (such as rock), when they have a nonspherical shape or when multiple particles interact with the sensor at the same time. However, two major components of error will dominate the field measurements. The first is the integrated calibration equation for the whole sensor plate (equation 6). To check this equation directly, the impact strength and location for every bed load particle passing the plate would need to be known, which is difficult even in the laboratory and hardly possible in a field situation. The second is the assumption that all parts of the sensor plate are impacted by moving particles at an equal rate. For the various regions of the sensor plate, the sensor output differs by a factor of up to five for the same delivered energy (cf. Figure 4), and clearly, this affects measurement accuracy. At the Erlenbach, measurement intervals are set to 1 min, and it seems unlikely that all possible combinations of grain size impact location and corresponding impact energies are realized within this time frame. The situation is somewhat better for the other streams, where data are recorded in 10 or 15 min intervals. A direct measurement of impact locations and local impact energies and thus a formal error analysis is currently not possible. We set the error in the energy measurements to 30%, for the purpose of this paper. The value is derived from the long-term experience of working with the sensor system and seems to provide a reasonable error estimate. A more thorough approach needs further laboratory and field experiments and is left for future studies.

5.2. Energy Delivery to the Bed

[30] Energy is delivered to the bed mainly due to impacts of bed load particles [cf. *Hartshorn et al*., 2002; *Sklar and Dietrich*, 2004; *Burtin et al*., 2008; *Turowski et al*., 2008b]. Indeed, in the October event, delivered energy E_{bed} is correlated to the bed load transport rates with a nearly linear dependence (Figure 10). However, some caution needs to be applied in the interpretation of these data, since in our experiments, both the energy delivered to the bed and the bed load transport rates have been measured with the same instrument. For a given transport rate, large scatter up to an order of magnitude can be observed. Bed load transport rates are known to fluctuate over several orders of magnitude even for constant discharge (Figure 7c). There are several reasons for this fluctuation, including the availability of sediment, spatially and temporarily varying grain size distributions and grain shape, the motion of bed forms, and turbulent force fluctuations in the water [e.g., *Hoey*, 1992; *Chen and Stone*, 2008; *Turowski*, 2010]. Thus, the same transport rate may have been recorded at very different discharges, corresponding to different grain sizes and grain velocities, which can ultimately result in different energy delivery. In addition, a bed load particle of a given size can deliver varying amounts of energy to the bed, depending on its mode of transport (rolling, sliding, saltating), its shape, its velocity, and on the characteristics of motion immediately before and during the impact [cf. *Turowski and Rickenmann*, 2009]. A further source of the scatter may be the changing grain size distribution: The same transport rates can result from a small number of large particles crossing the sensor or a large number of small particles, which may result in different sensor signals [cf. *Rickenmann et al*., 2013]. Similar considerations can explain the scatter observed in the energy-delivery ratio (Figure 7b).

5.3. Prediction of the Energy Delivered to the Bed Using the Saltation-Abrasion Model and Empirical Equations

[31] With method 1, using the measured bed load transport rates in equation (8), calculated energies overestimate measured energies on average by a factor of 32 (Figure 11a). Part of the observed shift is due to the different definition of energy in measurement (energy delivered to the bed) and calculation (impactor kinetic energy upon impact). However, it seems unlikely that only ~3% of the energy of the impactor is ultimately delivered to the bed. In the laboratory experiments used for calibration (see section 3.1), about 40% of the kinetic energy of the impactor was passed onto the sensor plate while about 60% was retained in the rebound. There, a rubber ball with a steel core was used to impact the sensor unit's steel plate. We expect that a higher fraction is passed to the bed for impacts of rock on rock, since the geophone sensors are covered by steel plates mounted on elastomers, giving a stronger elastic response and thus higher rebound heights than bedrock. Part of the overestimation is thus likely to be due to the model formulation, for example, due to the inadequate description of saltation trajectories [cf. *Chatanantavet et al*., 2013].

[32] Using method 2, where bed load transport rates were calculated with the calibrated equation of *Barry et al*. [2004], calculated energies overestimate measured energies

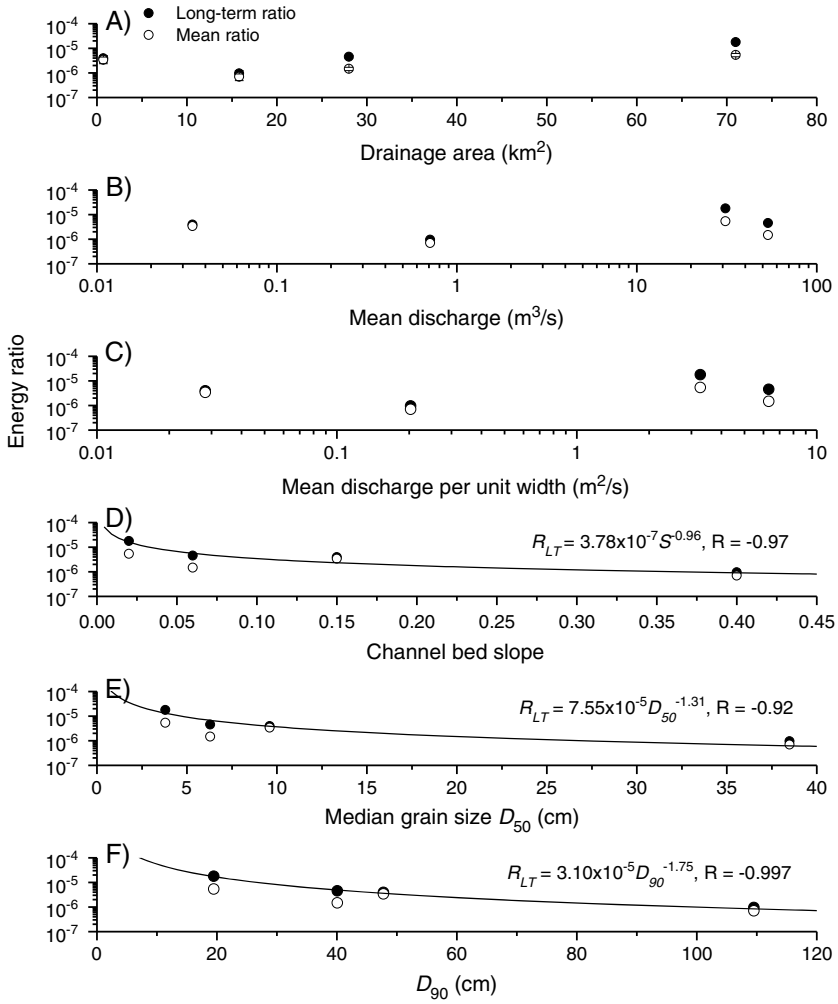

Figure 9. Long term and mean ratios of the energy delivered to the bed to the total stream energy, shown as function of (a) drainage area, (b) mean discharge calculated for the periods under consideration, (c) mean discharge normalized by channel width, (d) channel bed slope, (e) median grain size, and (f) the 90th percentile of the grain size distribution. The regression lines shown in Figures 9d–9f are all for the long-term ratio R_{LT}.

on average by a factor of about 138 (Figure 11b). There is a strong trend in this overestimation; at small transport rates, the overestimation can exceed 2 orders of magnitude; at higher transport rates, calculations draw nearer to the observations. A reason for the poor performance may be well-known problems of bed load transport prediction at steep slopes, which is usually put down to macroroughness in the stream and limited sediment availability [e.g., *Nitsche et al.*, 2011; *Yager et al.*, 2007, 2012]. However, note that we calibrated the equation used in method 2 to the long-term sediment yield of the Erlenbach, and nonlinear averaging effects probably dominate the difference between observed and predicted energy. The results suggest that in the near future, it may be difficult to predict the energy delivered to the bed with laboratory-developed empirical equations similar to bed load transport models. Not only do we need (as of today very uncertain) transport predictions for this task, but there are additional sources of scatter, which are only incompletely understood (see section 5.2). In addition, obtaining high-quality field data is difficult and expensive, and the available database will likely expand only slowly.

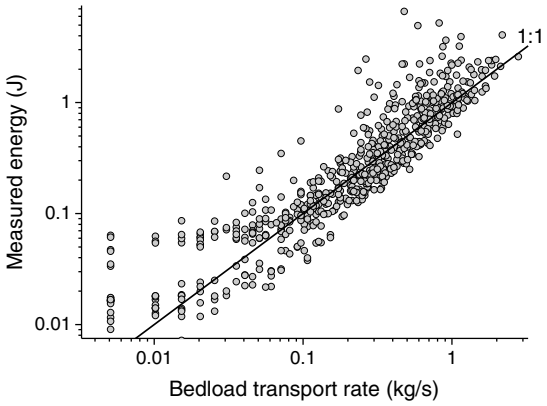

Figure 10. Measured energy delivered to the bed as function of bed load transport rates for the October 2011 event at the Erlenbach. A clear trend is visible, but data scatter over up to an order of magnitude for a given transport rate. Note, however, that the data are not independent, since values on both axes are derived from measurements with the geophone system.

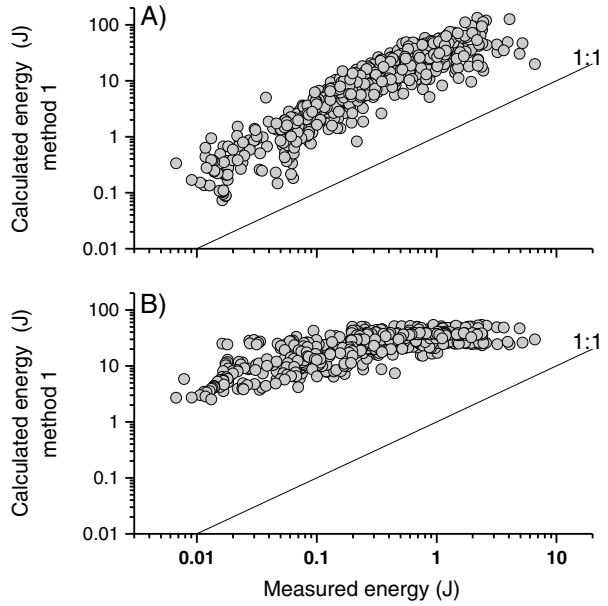

Figure 11. Calculated and measured energies for the October event at the Erlenbach. (a) Impactor energies calculated with method 1, using measured bed load transport rates. (b) Impactor energies calculated with method 2, using an empirical bed load transport model.

[33] As another possible empirical approach, we can relate the energy delivered to the bed to the stream hydraulics directly (Figure 7a). These data, too, show considerable scatter. For the October event, a good fit is obtained using both a power law and an exponential model (Figure 12a). For the complete monitoring period, scatter is considerably larger, but the regression lines give a similarly good fit to the mean trend (Figure 12b). However, it is clear from Figure 8 that the Erlenbach equation will not fit the data from the other three streams. Currently, it is not possible to derive a general relationship, but site-specific relations might be feasible with broader data sets.

5.4. Control of Catchment Parameters and Empirical Erosion Models

[34] Our sensor measures the energy transferred to them by passing bed load. This is an analogy to fundamental assumptions in bedrock erosion models. Although we do not measure energy transfer to a bedrock bed, and although all the streams we have data feature an alluvial bed, we can use the data to make inferences about bedrock erosion, as the steel plate covering the sensor units is similarly smooth as bedrock polished by erosive action. We expect the fraction of energy delivered to the bed by moving bed load to be a function of stream bed roughness. Roughness will affect energy dissipation in the stream and thus modulate the energy available for sediment transport [e.g., *Yager et al*., 2007; *Nitsche et al*., 2011]. This again would lead to a reduction in energy delivered to the bed by moving bed load with increasing roughness. In addition, roughness will affect the type of motion of the particles (rolling, sliding, saltation), which in turn will determine the energy delivered to the bed [cf. *Turowski and Rickenmann*, 2009]. This could lead both to a reduction (decreased particle velocity) or an increase (more frequent bed contacts and thus higher cumulative impact energies) in the energy delivered to the bed with increasing roughness. Typically, slope is well correlated with roughness [e.g., *Nitsche et al*., 2012] and can be used as a proxy. In addition, slope directly affects delivered energies, since it modulates the partitioning of the impact energy in bed-normal and bed-parallel components, and, in addition, it is used to calculate total stream energy (equation 7). Characteristic grain sizes such as D_{50} or D_{90} are often used to quantify roughness or to evaluate roughness coefficients [e.g., *Ferguson*, 1994; *Rickenmann and Recking*, 2011; *Nitsche et al*., 2012]. We find a negative correlation with all three of these parameters (slope, D_{50}, D_{90}; Figures 9d–9f). The exponent of near minus one in the relationship between R_{LT} and slope implies that the energy delivered to the bed is approximately independent of slope, since there is a linear dependency of stream power on slope (equation 7).

[35] We note that the correlations based on only four data points are not very satisfactory. In addition, the measurement

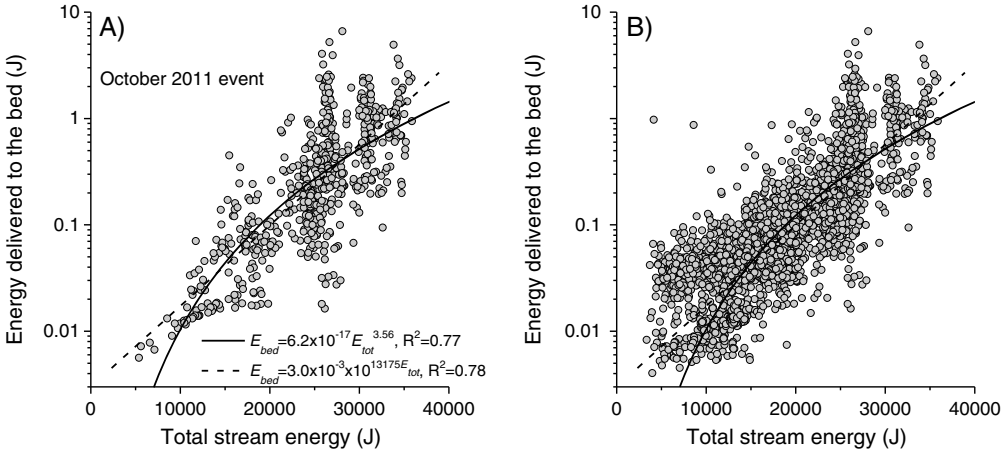

Figure 12. (a) Energy delivered to the bed as function of total stream energy for the October 2011 event in the Erlenbach. Both power law and exponential fits give a reasonable description of the data. (b) The same relation for whole monitoring period in the Erlenbach. The regression lines are the same as in Figure 12a. The same data are plotted on double-logarithmic axes in Figure 8a.

Table 2. Regression Coefficients for the Empirical Erosion Models (see Figure 9)

Parameter	Prefactor c	Exponent α	Goodness of fit R
Slope S	3.78×10^{-7}	−0.96	−0.97
D_{50} (cm)	7.55×10^{-5}	−1.31	−0.92
D_{90} (cm)	3.10×10^{-5}	−1.75	−0.997

periods for some of the streams span only a few months. But we can use the regression equations shown in Figure 9 to construct tentative preliminary empirical long-term erosion models, based on channel bed slope and grain size characteristics.

$$R_{\mathrm{LT}} = \frac{E_{\mathrm{bed}}}{E_{\mathrm{tot}}} = cX^{\alpha} \tag{12}$$

[36] Here X stands for any of the three parameters (S, D_{50}, D_{90}), and c and α are the parameters obtained from the regressions (Table 2 and Figure 9). Multiplying equation 2 with the particle impact rate I_r to obtain incision rates I, we can write

$$I = V_i I_r = \frac{E_{\mathrm{bed}}}{E_V} = c\frac{E_{\mathrm{tot}}}{E_V}X^{\alpha} \tag{13}$$

[37] Here the energy delivered in a single impact E_g has been replaced by the cumulative delivered energy E_{bed}. According to *Sklar and Dietrich* [2004, equation (4)], the energy per unit volume needed to remove the rock ε_v is a function of the rock's properties:

$$\varepsilon_v = \frac{k_v \sigma_T^2}{2Y} \tag{14}$$

[38] Here σ_T is the tensile strength of the rock, Y its Young's modulus, and k_v is a dimensionless rock resistance coefficient. The coefficient not only subsumes the erosion efficiency but is also dependent on bed load properties. For example, the coefficient includes the factor describing the proportion of energy that is actually delivered to the bed out of the total kinetic energy of the impactor upon impact. We can write

$$E_V = \kappa \varepsilon_v \tag{15}$$

[39] Here κ is a dimensionless constant denoting the fraction of total kinetic energy actually delivered to the bed upon impact. Substituting equations (7), (14), and (15) into equation (13), the incision rate I can be written as

$$I = c\frac{2Yg\rho\langle Q\rangle S}{\kappa k_v \sigma_T^2}X^{\alpha} \tag{16}$$

[40] Here $< Q >$ denotes the time-averaged discharge. Equation (16) was derived using the long-term energy-delivery ratio and is therefore not a process law. It is not suitable to model instantaneous bedrock incision, but it can be used in landscape evolution models featuring time steps longer than several months.

[41] We can use equation (16) to attempt to bridge the gap between our empirical results and a popular family of erosion models, the stream power law. The stream power model for bedrock incision has been proposed by *Seidl et al*. [1994] and has since been widely used to calculate fluvial bedrock erosion in landscape or channel evolution models [e.g., *Tucker and Slingerland*, 1994; *Crave and Davy*, 2001; *Lague*, 2010; *Braun and Willett*, 2013]. In the stream power model, incision rate I is expressed as a power function of discharge Q (or, alternatively, drainage area) and channel bed slope S:

$$I = k_e Q^m S^n \tag{17}$$

[42] Here k_e is a coefficient describing the erodibility of the bedrock. A model similar to equation (17) can be derived from the assumption that bedrock incision is a function of bed shear stress [*Howard and Kerby*, 1983]. The slope exponent n has been argued to depend on the dominant incision process, and to take a value between $\frac{2}{3}$ and $\frac{5}{3}$ [*Whipple et al*., 2000], while the ratio m/n should be around $\frac{1}{2}$ [e.g., *Whipple and Tucker*, 1999].

[43] The similarity of equations (16) and (17) is obvious. The ratio m/n, which is expected to equal ~0.5 from channel long-profile analysis [e.g., *Whipple and Tucker*, 1999] would, according to our data, be equal to one if D_{50} or D_{90} are used in place of X or approach a very large value if slope is used instead of X (cf. Table 2). Several reasons may be put forward to account for this discrepancy. First, the fraction of E_{kin} delivered to the bed (denoted by κ) may be slope dependent, altering the dependence on slope in the whole relation. We have so far only rough constraints on this parameter using field data from the Erlenbach (see section 5.3). Second, the rock resistance parameter k_v, a laboratory-calibrated scaling factor in the saltation-abrasion model [*Sklar and Dietrich*, 2004] can be expected to be site dependent, as it subsumes details of the impact and rebound, and of energy-delivery processes. An implicit or explicit slope dependency cannot currently be ruled out. Third, averaging discharge over longer time periods may lead to nonlinear effects that may introduce a slope dependency [cf. *Lague et al*., 2005]. For instance, it has been shown that discharge variability is dependent on drainage area and therefore implicitly on slope [*Molnar et al*., 2006]. Fourth, it needs to be noted here that in our analysis, so far, the cover effect term F_e [cf. *Sklar and Dietrich*, 2004, equation (1)] has been neglected and needs to be multiplied onto equation (16) for use in sediment-rich channels:

$$I = c\frac{2Yg\rho\langle Q\rangle S}{\kappa k_v \sigma_T^2}X^{\alpha}F_e \tag{18}$$

[44] The cover effect arises due to the protection of the bed from impacting particles offered by sediment residing on it [*Gilbert*, 1877; *Sklar and Dietrich*, 2004]. Typically, the cover effect is written as a function of the ratio of sediment supply and transport capacity, which are dependent on both discharge and slope [cf. *Sklar and Dietrich*, 2004; *Turowski et al*., 2007; *Hodge and Hoey*, 2012]. Thus, clearly, the relationship between incision rate, discharge, and slope changes when the cover effect is taken into account. Our

observations, encapsulated in equation (18), therefore, tentatively suggest that a version of the stream power law that includes the cover effect can adequately describe long-term bedrock incision in mountain streams. The dynamics of such a function and its implications for the channel long-profile, for transient incision, and for landscape evolution have for example been investigated by *Gasparini et al*. [2006, 2007], *Lague* [2010], and *Whipple and Tucker* [2002].

6. Conclusion

[45] Field measurements of the energy delivered to the bed are possible in mountain streams using impact plates equipped with geophones originally designed for the monitoring of bed load transport [*Rickenmann and McArdell*, 2007; *Rickenmann et al*., 2012]. We have calibrated this sensor system with laboratory experiments to absolute energy values and applied this method of analysis in four mountain streams in Austria and Switzerland. Unsurprisingly, delivered energy displays similar characteristics as are known for bed load transport rates in mountain streams. These include a strong dependence on discharge and a large scatter for a given discharge. Predictive empirical equations can be derived with a similar accuracy as empirical bed load transport models. However, such equations are site specific, and with data from only four streams, it is currently impossible to derive a model with general validity. The sensor system used in our study is installed in several other streams beside the ones that we studied here [e.g., *Turowski et al*., 2008a, *Rickenmann et al*., 2013], and although data on the squared integrals are currently not available for all of them, these systems may be upgraded in the future to record this parameter.

[46] The direct measurement of the energy delivered to the bed is advantageous in several respects. Existing mechanistic erosion models, chiefly the saltation-abrasion model [*Sklar and Dietrich*, 2004] and its derivatives [*Lamb et al*., 2008; *Chatanantavet and Parker*, 2009], rely on theoretical, semi-empirical or empirical relationships that are usually calibrated on laboratory data recorded in conditions that are insufficiently representative of those observed in natural mountain streams. A comparison of our field data with calculations using an equation that is a component of the saltation-abrasion model reveals that measured bed load transport rates need to be available to reliably predict the trends of energy delivery (and thus bedrock erosion rates) observed in nature. Even so, calculated energy delivery overestimates measured values. With measurements of the energy delivered to the bed in natural mountain streams such as reported here, some of the assumptions and components of mechanistic erosion models can be evaluated directly against field data. In addition, field-derived empirical relationships for the energy delivery to the bed significantly reduce the number of assumptions that need to be made to arrive at a usable erosion model.

[47] We have found relationships between the fraction of the total energy delivered to the bed and the channel bed slope or characteristic grain sizes of the channel bed. If these relationships can be substantiated, they may provide links between the local process of bedrock erosion and incision models upscaled to the reach. This may help to explain the large success the stream power model family has enjoyed in the landscape evolution community [e.g., *Whipple and Tucker*, 1999, 2002; *Braun and Willett*, 2013], despite the fact that it tends to fail to describe observation when it is used as a process law or when sediment effects are taken into account [*Sklar and Dietrich*, 2001; *Johnson and Whipple*, 2007; *Turowski et al*., 2008b; *Yanites and Tucker*, 2010; *Cook et al*., 2013].

Notation

B	magnetic flux density (T)
c	power law regression coefficient, variable units
d	distance between the magnetic poles (m)
D_{50}	median grain size (m)
D_{90}	90th percentile of the grain size distribution (m)
E_{bed}	energy delivered to the channel bed (J)
E_{g}	energy delivered to the channel bed by a single impact (J)
E_{kin}	kinetic energy of the impactor at the moment of impact (J)
E_{tot}	total stream energy (J)
$E_{\mathrm{V}}\,E_{\mathrm{bed}}$	per unit volume needed to erode the rock (J m^{-3})
F_e	cover term
g	gravitational acceleration at the Earth's surface (m s^{-2})
H	Hydraulic radius (m)
h	rebound height (m)
I	incision rate (m s^{-1})
I_r	particle impact rate (m^{-2} s^{-1})
k_B	prefactor of the bed load transport equation (m$^{3(1-\beta)}$ s$^{\beta-1}$)
k_e	rock erodibility coefficient
k_v	rock resistance coefficient
K	calibration constant
L	length of the geophone plate (= 0.36 m) (m)
m	discharge exponent in the stream power model
M_{imp}	impactor mass (kg)
n	slope exponent in the stream power model
q^*	dimensionless bed load transport ratio
q_s	bed load transport rate per unit width (kg s^{-1} m^{-1})
Q	discharge (m^3 s^{-1})
Q_s	bed load transport rate (kg s^{-1})
$<Q>$	time-averaged discharge (m^3 s^{-1})
R	energy-delivery ratio, $R = E_{\mathrm{bed}}/E_{\mathrm{tot}}$
R_{LT}	long-term energy-delivery ratio
R_M	mean energy-delivery ratio
S	channel bed slope
Δt	time interval (s)
U_g	sensor voltage (V)
U_{ind}	voltage induced in the coil (V)
v	velocity of the permanent magnet (m s^{-1})
V_i	average volume of rock removed by a single particle impact (m^3)
V_{imp}	impactor velocity at the moment of impact (m s^{-1})
X	place holder parameter used for D_{50}, D_{90}, or S
Y	Young's modulus of the rock (Pa)
α	power law regression exponent
β	exponent of the bed load transport equation
ε_t	impact energy threshold for erosion (J)
$\varepsilon_v\,E_{\mathrm{kin}}$	per unit volume needed to erode the rock (J m^{-3})
ρ	density of water (kg m^{-3})
ρ_s	density of sediment (kg m^{-3})

κ fraction of impactor kinetic energy delivered to the bed, $\kappa = E_{\mathrm{bed}}/E_{\mathrm{kin}}$
σ_T tensile strength of the rock (Pa)
τ bed shear stress (Pa)
τ_c critical bed shear stress for the onset of bed load motion (Pa)
$\tau_{d_{50s}}$ critical bed shear stress for the median grain size at the surface (Pa)
$\tau_{d_{50ss}}$ critical bed shear stress for the median grain size of the subsurface (Pa)
τ_{Q_2} bed shear stress for the 2 year flood (Pa)
Ω stream power (J m^{-1} s^{-1})

[48] **Acknowledgments.** We thank R. Boes and D. Felix for discussions. B. Fritschi built and maintained the measurement systems used here. The TIWAG water power company maintains the Austrian observation sites (Fischbach, Ruetz) and kindly provided data. The Mattmark water power company maintains the site at the Riedbach and supported the measurement campaign. J. Schneider provided additional information on the Riedbach channel and catchment. We are grateful to AE N. Gasparini, to P. Chatanantavet, and an anonymous reviewer for their comments. This study was supported by SNF grants 200021_137681/1 and 200021_132163/1 and by WSL.

References

Barry, J. J., J. M. Buffington, and J. G. King (2004), A general power equation for predicting bed load transport rates in gravel bed rivers, *Water Resour. Res.*, *40*, W10401, doi:10.1029/2004WR003190.

Barry, J. J., J. M. Buffington, and J. G. King (2007), Correction to "A general power equation for predicting bed load transport rates in gravel bed rivers", *Water Resour. Res.*, *43*, W08702, doi:10.1029/2007WR006103.

Bitter, J. G. A. (1963a), A study of erosion phenomena, Part I, *Wear*, *6*, 5–21.

Bitter, J. G. A. (1963b), A study of erosion phenomena, Part II, *Wear*, *6*, 169–190.

Böckli, M. (2011). Laborversuche zum Verhalten von Geophon-Sensoren. Master's thesis, ETH Zürich and WSL, 56 p.

Braun, J., and S. D. Willett (2013), A very efficient *O*(*n*), implicit and parallel method to solve the stream power equation governing fluvial incision and landscape evolution, *Geomorphology*, *180–181*, 170–179, doi:10.1016/j.geomorph.2012.10.008.

Burtin, A., L. Bollinger, J. Vergne, R. Cattin, and J. L. Nábělek (2008), Spectral analysis of seismic noise induced by rivers: A new tool to monitor spatiotemporal changes in stream hydrodynamics, *J. Geophys. Res.*, *113*, B05301, doi:10.1029/2007JB005034.

Chatanantavet, P., and G. Parker (2009), Physically-based modeling of bedrock incision by abrasion, plucking, and macroabrasion, *J. Geophys. Res.*, *114*, F04018, doi:10.1029/2008JF001044.

Chatanantavet, P., K. X. Whipple, M. A. Adams, and M. P. Lamb (2013), Experimental study on coarse grain saltation dynamics in bedrock channels, *J. Geophys. Res. Earth Surface*, *118*, 1–16, doi:10.1002/jgrf.20053.

Chen, L., and M. C. Stone (2008), Influence of bed material size heterogeneity on bed load transport uncertainty, *Water Resour. Res.*, *44*, W01405, doi:10.1029/2006WR005483.

Cook, K., J. M. Turowski, and N. Hovius (2013), A demonstration of the importance of bed load transport for fluvial bedrock erosion and knickpoint propagation, *Earth Surf. Process. Landforms*, *38*, 683–695, doi:10.1002/esp.3313.

Crave, A., and P. Davy (2001), A stochastic precipiton model for simulating erosion/sedimentation dynamics, *Comput. Geosci.*, *27*, 815–827.

Egholm, D. L., M. F. Knudsen, and M. Sandiford (2013), Lifespan of mountain ranges scaled by feedbacks between landsliding and erosion by rivers, *Nature*, *498*, 475–478, doi:10.1038/nature12218.

Fehr, R. (1987), Einfache Bestimmung der Korngrössenverteilung von Geschiebematerial, *Schweiz. Ing. und Architekt*, *105*(38), 1004–1109.

Ferguson, R. I. (1994), Critical discharge for entrainment of poorly sorted gravel, *Earth Surf. Process. Landforms*, *19*, 179–186, doi:10.1002/esp.3290190208.

Gasparini, N. M., K. X. Whipple, and R. L. Bras (2006). Numerical modeling of non-steady-state river profile evolution using a sediment-flux-dependent incision model, in *Tectonics, Climate, and Landscape Evolution*, Geological Society of America Special Paper Penrose Conference Series, vol. 398, edited by S. D. Willett, N. Hovius, M. T. Brandon, and D. M. Fisher, pp. 127–141, Geological Society of America, Boulder, Colorado, USA, doi:10.1130/2006.2398(08).

Gasparini, N. M., K. X. Whipple, and R. L. Bras (2007), Predictions of steady state and transient landscape morphology using sediment-flux-dependent river incision models, *J. Geophys. Res.*, *112*, F03S09, doi:10.1029/2006JF000567.

Gilbert, G. K. (1877), Land sculpture, in *The Geology of the Henry Mountains*, vol. 167, edited by C. B. Hunt, chap. 5, pp. 99–150, Mem. Geol. Soc. Am., Utah.

Gray J. R., J. B. Laronne, and J. D. G. Marr (2010), Bed load-surrogate monitoring technologies. U.S. Geological Survey Scientific Investigations Report 2010–5091. http://pubs.usgs.gov/sir/2010/5091/.

Hartshorn, K., N. Hovius, W. B. Dade, and R. L. Slingerland (2002), Climate-driven bedrock incision in an active mountain belt, *Science*, *297*, 2036–2038.

Hasslacher, P., and C. Lanegger (1988), Österreichisches Gletscherbachinventar, Fachbeiträge des Oesterreichischen Alpenvereins, Alpine Raumverordnung 1, Österreichischer Alpenverein, Innsbruck, Austria.

Head, W. J., and M. E. Harr (1970), The development of a model to predict the erosion of materials by natural contaminants, *Wear*, *15*, 1–46.

Hegg, C., B. W. McArdell, and A. Badoux (2006), One hundred years of mountain hydrology in Switzerland by the WSL, *Hydrol. Process.*, *20*, 371–376, doi:10.1002/hyp.6055.

Hodge, R. A., and T. B. Hoey (2012), Upscaling from grain-scale processes to alleviation in bedrock channels using a cellular automaton model, *J. Geophys. Res.*, *117*, F01017, doi:10.1029/2011JF002145.

Hoey, T. (1992), Temporal variations in bed load transport rates and sediment storage in gravel-bed rivers, *Prog. Phys. Geogr.*, *16*, 319–338.

Hovius, N., and C. P. Stark (2006), Landslide-driven erosion and topographic evolution of active mountain belts, in *Landslides From Massive Rock Slope Failure*, edited by S. G. Evans, G. S. Mugnozza, A. Strom, and R. L. Hermanns, pp. 573–590, Springer, Dordrecht, Netherlands.

Howard, A. D., and G. Kerby (1983), Channel changes in badlands, *Geol. Soc. Am. Bull.*, *94*, 739–752.

Johnson, J. P., and K. X. Whipple (2007), Feedbacks between erosion and sediment transport in experimental bedrock channels, *Earth Surf. Process. Landforms*, *32*, 1048–1062, doi:10.1002/esp.1471.

Johnson, J. P., and K. X. Whipple (2010), Evaluating the controls of shear stress, sediment supply, alluvial cover, and channel morphology on experimental bedrock incision rate, *J. Geophys. Res.*, *115*, F02018, doi:10.1029/2009JF001335.

Lague, D. (2010), Reduction of long-term bedrock incision efficiency by short-term alluvial cover intermittency, *J. Geophys. Res.*, *115*, F02011, doi:10.1029/2008JF001210.

Lague, D., N. Hovius, and P. Davy (2005), Discharge, discharge variability and the bedrock channel profile, *J. Geophys. Res.*, *110*, F04006, doi:10.1029/2004JF000259.

Lamb, M. P., W. E. Dietrich, and L. S. Sklar (2008), A model for fluvial bedrock incision by impacting suspended and bed load sediment, *J. Geophys. Res.*, *113*, F03025, doi:10.1029/2007JF000915.

Molnar, P., R. S. Anderson, G. Kier, and J. Rose (2006), Relationships among probability Distributions of stream discharges in floods, climate, bed load transport, and river incision, *J. Geophys. Res.*, *111*, F02001, doi:10.1029/2005JF000310.

Momber, A. W. (2004), Wear of rocks by water flow, *Int. J. Rock Mech. Min. Sci.*, *41*, 51–68.

Moore, R. C. (1926), Origin of inclosed meanders on streams of the Colorado Plateau, *J. Geol.*, *34*, 29–57.

Nitsche, M., D. Rickenmann, J. M. Turowski, A. Badoux, and J. W. Kirchner (2011), Evaluation of bed load transport predictions using flow resistance equations to account for macro-roughness in steep mountain streams, *Water Resour. Res.*, *47*, W08513, doi:10.1029/2011WR010645.

Nitsche, M., D. Rickenmann, J. W. Kirchner, J. M. Turowski, and A. Badoux (2012), Macro roughness and between-site variations of flow resistance in steep mountain streams, *Water Resour. Res.*, *48*, W12518, doi:10.1029/2012WR012091.

Rickenmann, D., and B. W. McArdell (2007), Continuous measurement of sediment transport in the Erlenbach stream using piezoelectric bed load impact sensors, *Earth Surf. Process. Landforms*, *32*, 1362–1378, doi:10.1002/esp.1478.

Rickenmann, D., and B. W. McArdell (2008), Calibration of piezoelectric bed load impact sensors in the Pitzbach mountain stream, *Geodin. Acta*, *21*, 35–52, doi:10.3166/ga.21.35-52.

Rickenmann, D., and A. Recking (2011), Evaluation of flow resistance in gravel-bed rivers through a large field data set, *Water Resour. Res.*, *47*, W07538, doi:10.1029/2010WR009793.

Rickenmann, D., J. M. Turowski, B. Fritschi, A. Klaiber, and A. Ludwig (2012), Bed load transport measurements at the Erlenbach stream with geophones and automated basket samplers, *Earth Surf. Process. Landforms*, *37*, 1000–1011, doi:10.1002/esp.3225.

Rickenmann, D., J. M. Turowski, B. Fritschi, J. Laronne, R. Barzilai, I. Reid, A. Kreisler, J. Aigner, H. Seitz, and H. Habersack (2013), Bed load transport measurements with impact plate geophones: Comparison of

sensor calibration at different gravel-bed streams, *Earth Surf. Process. Landforms*, doi:10.1002/esp.3499, in press.

Seidl, M. A., W. E. Dietrich, and J. W. Kirchner (1994), Longitudinal profile development into bedrock: An analysis of Hawaiian channels, *J. Geol.*, *102*, 457–474.

Sklar, L. S., and W. E. Dietrich (2001), Sediment and rock strength controls on river incision into bedrock, *Geology*, *29*, 1087–1090, doi:10.1130/0091-7613(2001)029<1087:SARSCO>2.0.CO;2.

Sklar, L. S., and W. E. Dietrich (2004), A mechanistic model for river incision into bedrock by saltating bed load, *Water Resour. Res.*, *40*, W06301, doi:10.1029/2003WR002496.

Tucker, G., and R. Slingerland (1994), Erosional dynamics, flexural isostacy, and long-lived escarpments: A numerical modeling study, *J. Geophys. Res.*, *99*, 12,229–12,243.

Turowski, J. M. (2010), Probability distributions of bed load transport rates: A new derivation and comparison with field data, *Water Resour. Res.*, *46*, W08501, doi:10.1029/2008WR008488.

Turowski, J. M. (2012), Semi-alluvial channels and sediment-flux-driven bedrock erosion, Chapter 29 in *Gravel Bed Rivers: Processes, Tools, Environments*, edited by M. Church, P. Biron, and A. Roy, pp. 401–416, JohnWiley & Sons, Chichester, doi:10.1002/9781119952497.

Turowski, J. M., and D. Rickenmann (2009), Tools and cover effects in bed load transport observations in the Pitzbach Austria, *Earth Surf. Process. Landforms*, *34*, 26–37, doi:10.1002/esp.1686.

Turowski, J. M., and D. Rickenmann (2011), Measuring the statistics of bed load transport using indirect sensors, *J. Hydrol. Eng.*, *137*, 116–121, doi:10.1061/(ASCE)HY.1943-7900.0000277.

Turowski, J. M., D. Lague, and N. Hovius (2007), Cover effect in bedrock abrasion: A new derivation and its implications for the modeling of bedrock channel morphology, *J. Geophys. Res.*, *112*, F04006, doi:10.1029/2006JF000697.

Turowski, J. M., A. Badoux, D. Rickenmann, and B. Fritschi (2008a), Erfassung des Sedimenttransportes in Wildbächen und Gebirgsflüssen—Anwendungsmöglichkeiten von Geophonmessanlagen, *Wasser Energ. Luft*, *100*, 69–74.

Turowski, J. M., N. Hovius, M.-L. Hsieh, D. Lague, and M.-C. Chen (2008b), Distribution of erosion across bedrock channels, *Earth Surf. Process. Landforms*, *33*, 353–363, doi:10.1002/esp.1559.

Turowski, J. M., E. M. Yager, A. Badoux, D. Rickenmann, and P. Molnar (2009), The impact of exceptional events on erosion, bed load transport and channel stability in a step-pool channel, *Earth Surf. Process. Landforms*, *34*, 1661–1673, doi:10.1002/esp.1855.

Turowski, J. M., A. Badoux, and D. Rickenmann (2011), Start and end of bedload transport in gravel bed rivers, *Geophys. Res. Lett.*, *38*, L04401, doi:10.1029/2010GL046558.

Whipple, K. X., and G. E. Tucker (1999), Dynamics of the stream-power river incision model: Implications for height limits of mountain ranges, landscape response timescales, and research needs, *J. Geophys. Res.*, *104*, 17,661–17,674, doi:10.1029/1999JB900120.

Whipple, K. X., and G. E. Tucker (2002), Implications of sediment-flux-dependent river incision models for landscape evolution, *J. Geophys. Res.*, *107*, 2039, doi:10.1029/2000JB000044.

Whipple, K. X., G. S. Hancock, and R. S. Anderson (2000), River incision into bedrock: Mechanics and relative efficacy of plucking, abrasion, and cavitation, *Geol. Soc. Am. Bull.*, *112*, 490–503.

Wilson, A., N. Hovius, and J. M. Turowski (2013), Upstream facing convex surfaces: Bedrock bedforms produced by fluvial bed load abrasion, *Geomorphology*, *180–181*, 187–204, doi:10.1016/j.geomorph.2012.10.010.

Yager, E. M., J. W. Kirchner, and W. E. Dietrich (2007), Calculating bed load transport in steep boulder bed channels, *Water Resour. Res.*, *43*, W07418, doi:10.1029/2006WR005432.

Yager, E. M., J. M. Turowski, D. Rickenmann, and B. W. McArdell (2012), Sediment supply, grain protrusion, and bed load transport in mountain streams, *Geophys. Res. Lett.*, *39*, L10402, doi:10.1029/2012GL051654.

Yanites, B. J., and G. E. Tucker (2010), Controls and limits on bedrock channel geometry, *J. Geophys. Res.*, *115*, F04019, doi:10.1029/2009JF001601.